Millimeter-Wave Signal Properties Resulting From Electrooptical Upconversion

Konstantin Kojucharow, *Student Member, IEEE,* Michael Sauer, *Member, IEEE,* and Christian Schäffer, *Member, IEEE*

***Abstract*—This paper describes the combined effects of laser chirp, electrooptical mixing, dispersive fiber transmission, and photodetection on the nonlinear signal properties of the electrooptically generated millimeter-wave signal (60 GHz). Analytical expressions describing the complex currents of fundamental and higher order products are provided for the case of single-tone modulation as well as for two-tone modulation, respectively. Examples will be considered including the nonlinear amplitude response (output power at millimeter-wave range versus input power at IF), the nonlinear phase response (relative output phase at millimeter-wave range versus input power at IF), the input related 1-dB gain compression condition, the amplitude response of third- and fifth-order intermodulation products, as well as the input related intercept points for the latter signals. The model developed performed well, even under moderate to large signal conditions, and very good agreement has been achieved between theory and experiment.**

***Index Terms*—Dispersive optical channel propagation, electrooptical mixing, millimeter-wave communication, optical transmitter chirp.**

I. Introduction

THERE IS NOW greatly increased interest in commercial exploitation of the millimeter-wave region of the electromagnetic spectrum. The principal advantages offered by operation of systems at this range are the result of a wide fractional bandwidth, the short wavelength enabling high spatial resolution, and, finally, the reduced antenna dimensions. Furthermore, the still available spectrum has been drawing further attention. The high atmospheric attenuation in some regions of the spectrum can be turned to advantage to provide security to minimize interference within the system or between adjacent systems.

At millimeter-wave range, numerous picocells will have to be created within the communication system, requiring a high number of base stations to be connected to a central control station. This gives rise to new system design criteria, where simplicity of base station architecture and system flexibility are very important features. In order to reduce system complexity, the idea is to achieve all signal processing, oscillator generation, and system management in a central control station. The numerous base stations will then merely operate as remote transponders. Analog optical links will offer a powerful means to achieve this function.

Manuscript received January 5, 2001; revised May 25, 2001.

K. Kojucharow and C. Schäffer are with the Communications Laboratory, Dresden University of Technology, D-01062 Dresden, Germany.

M. Sauer was with the Communications Laboratory, Dresden University of Technology, D-01062 Dresden, Germany. He is now with Corning Inc., Corning, NY 14831 USA.

Publisher Item Identifier S 0018-9480(01)08720-8.

Different methods for feeding the remote transponders with optical millimeter-wave signals have been proposed and demonstrated, such as optical self-heterodyne techniques [1]–[3], external modulation [4], electrical and optical frequency conversion techniques [5], [6], and electrooptical transceiver techniques [7], [8]. In [9], we proposed and demonstrated a system concept where a Ka-band master oscillator was simultaneously imposed onto the optical channels of a dense wavelength division multiplex (DWDM) system by means of a single external electrooptical modulator (EOM). All IF signals, which are directly modulating the laser diodes, are electrooptically upconverted to the millimeter range. The complexity of the transponders can thus be significantly reduced.

In this paper, the electrical signal properties resulting from the electrooptical upconversion process are investigated including single-tone and two-tone modulation of the laser diode. After developing analytical expressions for the received signal in amplitude and phase, we discuss examples and compare measurements with calculated results. The very good agreement between measurement and developed theory is demonstrated.

II. Analyzed Topology

In this paper, a detailed derivation of *electrical* end-to-end transmission properties of the optical subsystem for the case of the electrooptical upconversion will be provided. Bridging between the system considerations and the mathematical description, Fig. 1 illustrates the cascade of components through which a signal will be passing when traveling from the central control station toward the air interface. The downlink path will be considered in the following. Based on this, a model for the single optical channel upconversion process has been defined. Fig. 2 depicts the configuration of the analyzed subsystem. Wavelength division multiplexing (WDM) is excluded since its influence on the (narrow IF range) laser diode spectrum is negligible. The WDM–demultiplexing elements do not appear in the model as such. Instead, a two-port optical bandpass channel filter is incorporated with an arbitrary frequency response identical to that of the to-be-used demultiplexers. Optical amplification has also been excluded at this point. Subsystem description begins with setting up the laser diode model for direct modulation conditions. Electrical single-tone as well as two-tone sine-wave modulation will be applied. The following steps include electrooptical mixing (Mach–Zehnder external optical modulator), dispersive fiber transmission, optical filtering, and photodetection.

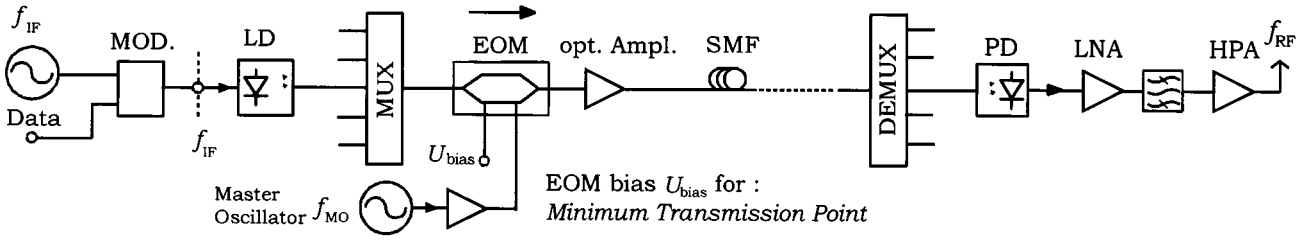

Fig. 1. Block diagram model of the downlink signal path (MOD: modulator; LD: laser diode; MUX: multiplexer; EOM: external optical modulator; SMF: single-mode fiber (optical backbone); DEMUX: demultiplexer; PD: photo diode (in the transponder).

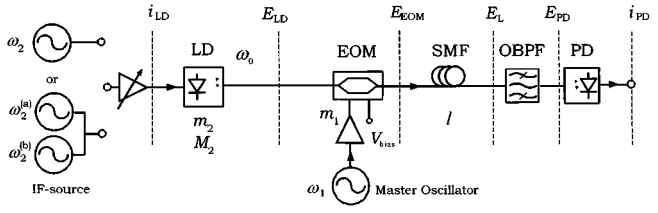

Fig. 2. Block diagram of the model utilized for calculation. OBPF: optical bandpass filter (as demux); the other components are the same as those in Fig. 1.

III. Derivation of the Combined IM-FM Spectrum/Laser Diode Model

A. Single-Tone Modulation

The laser diode is directly modulated by means of its bias current. It will exhibit intensity modulation (IM) as well as frequency modulation (FM) behavior (chirp). The optical spectrum of the laser diode, driven by a sinusoidal tone of variable magnitude, is based on a superposition of both modulation types and will be derived. Its time-dependent optical field can be written as

$$E_{\mathrm{LD}}(t) = E_1 \cdot \sqrt{1 + m_2 \sin(\omega_2 t + \Delta(\omega_2))} \cdot \exp j(\omega_0 t + M_2 \sin(\omega_2 t)) \quad (1)$$

where the factor E_1 is the optical field strength of the unmodulated device, the second factor represents the intensity modulation with m_2 as the IM index, and the third factor represents the frequency modulation contribution, with M_2 as the FM index. Further, ω_0, ω_2, and Δ denote angular optical emission frequency, the angular electrical modulation frequency, and the deviation angle between IM and FM, respectively [12], [14], [15]. A chirp factor $\alpha_{\mathrm{chirp}} = M_2(\omega_2)/m_2(\omega_2)$ can subsequently be used to substitute the FM index. The IM term has been expanded into a series [10]. Exclusion of cubic and higher order terms merely leads to an error in magnitude below 1% for all $m_2 < 0.65$. The exp-function (FM term) is first written in algebraic complex form and then expanded into a Fourier series [10]. The expanded FM term, developed up to the third term, is then combined with the IM term. It can be written after numerous algebraic manipulations as

$$\begin{aligned}\frac{E_{LD}(t)}{E_1} = &\left(1 - \frac{m^2}{16}\right) \sum_{n=-\infty}^{\infty} K_n e^{j(\omega_0 + n\omega_2)t} - j\,\frac{m_2}{4} \\ &\times \left\{ \sum_{n=-\infty}^{\infty} K_{n-1} e^{j(\omega_0 t + n\omega_2 t + \Delta)} \right. \\ &\left. - \sum_{n=-\infty}^{\infty} K_{n+1} e^{j(\omega_0 t + n\omega_2 t - \Delta)} \right\} \\ &+ \frac{m_2^2}{32} \left\{ \sum_{n=-\infty}^{\infty} K_{n-2} e^{j(\omega_0 t + n\omega_2 t + 2\Delta)} \right. \\ &\left. + \sum_{n=-\infty}^{\infty} K_{n+2} e^{j(\omega_0 t - n\omega_2 t - 2\Delta)} \right\} \quad (2)\end{aligned}$$

where the substitution $K_i = J_i(\alpha_{\mathrm{chirp}} m_2)$[1] and an abbreviation $\Delta = \Delta(\omega_2)$ are incorporated.

A term $\exp j(\omega_0 + n\omega_2)t$ can be separated next. Then, after several further steps, it can be written

$$E_{LD}(t) = E_1 \sum_{n=-\infty}^{\infty} L_n(m_2, \Delta) \exp j(\omega_0 + n\omega_2)t \quad (3)$$

which contains the important expression describing the complex envelope L of an arbitrary optical sideband

$$\begin{aligned}L_n(m_2, \Delta) = &\left\{ \left(1 - \frac{m_2^2}{16}\right) K_n + \frac{m_2}{4}(K_{n-1} + K_{n+1}) \sin\Delta \right. \\ &\left. + \frac{m_2^2}{32}(K_{n-2} + K_{n+2}) \cos 2\Delta \right\} \\ &+ j \left\{ -\frac{m_2}{4}(k_{n-1} - K_{n+1}) \cos\Delta \right. \\ &\left. + \frac{m_2^2}{32}(k_{n-2} - K_{n+2}) \sin 2\Delta \right\}. \quad (4)\end{aligned}$$

With the given model, one direct influence of the incorporated angle Δ can be observed in the asymmetrical optical spectrum,

[1]In order to avoid ambiguity with the Bessel function terms introduced by the Mach–Zehnder optical modulator (MZM) during the electrooptical upconversion process, the annotation K_i has been chosen for the Bessel functions of ith order and first kind. They are not to be confused with Bessel functions of ith order and second kind (*MacDonald* functions).

which is in accordance with [14] and [15]. For system considerations, the knowledge of this parameter within the operating frequency range of $\omega_{2\min} \le \omega_2 \le \omega_{2\max}$ is essential in order to predict photodetected currents of fundamental and higher order products precisely. Sensitivity of the calculation results to this parameter is highest in ranges where the detected millimeter-wave products show local minima in their dependence on fiber transmission length l or on laser electrical modulation power ($\sim m_2^2$), especially in the case of electrooptical upconversion. Uncertainty when omitting the Δ-parameter can reach several orders of magnitude in such dips and up to several decibels in other regions. Also, the nonlinear phase response is particularly affected by Δ; both effects will be shown later.

B. Two-Tone Modulation

The optical field at the output of the laser device can be written for this case

$$E_{LD}(t) = E_1 \cdot \sqrt{1 + m_2 \sin\left(\omega_2^{(a)} t + \Delta\right) + m_2 \sin\left(\omega_2^{(b)} t + \Delta\right)} \times \exp j\left(\omega_0 t + M_2 \sin\left(\omega_2^{(a)} t\right) + M_2 \sin\left(\omega_2^{(b)} t\right)\right) \tag{5}$$

where the modulation input currents at $\omega_2^{(a)}$ and $\omega_2^{(b)}$ are of equal magnitude. Their relative frequency separation is very small: the laser modulation slope will be $\eta_{LD}(\omega_2^{(a)}) \cong \eta_{LD}(\omega_2^{(b)})$ which leads to $m_2^{(a)} \cong m_2^{(b)} = m_2$, and subsequently to $M_2^{(a)} \cong M_2^{(b)} = M_2$ and $\Delta(\omega_2^{(a)}) = \Delta(\omega_2^{(b)}) \cong \Delta$. An identical approach has been applied to obtain the following expression for the optical field at the output of the laser diode:

$$\begin{aligned}\frac{E_{LD}(t)}{E_1} = {} & \sum_{m=-\infty}^{\infty}\sum_{n=-\infty}^{\infty} K_n K_m \cdot \exp j\left(\omega_0 + n\omega_2^{(a)} + m\omega_2^{(b)}\right)t + j\,\frac{m_2}{4} \\ & \cdot \left\{ \begin{aligned} & - \sum_{m=-\infty}^{\infty}\sum_{n=-\infty}^{\infty} K_{n-1} K_m \\ & \cdot \exp j\left(\omega_0 t + n\omega_2^{(a)} t + m\omega_2^{(b)} t + \Delta\right) \\ & + \sum_{m=-\infty}^{\infty}\sum_{n=-\infty}^{\infty} K_{n+1} K_m \\ & \cdot \exp j\left(\omega_0 t + n\omega_2^{(a)} t + m\omega_2^{(b)} t - \Delta\right) \\ & - \sum_{m=-\infty}^{\infty}\sum_{n=-\infty}^{\infty} K_n K_{m-1} \\ & \cdot \exp j\left(\omega_0 t + n\omega_2^{(a)} t + m\omega_2^{(b)} t + \Delta\right) \\ & + \sum_{m=-\infty}^{\infty}\sum_{n=-\infty}^{\infty} K_n K_{m+1} \\ & \cdot \exp j\left(\omega_0 t + n\omega_2^{(a)} t + m\omega_2^{(b)} t - \Delta\right) \end{aligned} \right\}. \end{aligned} \tag{6}$$

With the above expression, the complex envelope L of a specific product of angular frequency $\omega_0 + n\omega_2^{(a)} + m\omega_2^{(b)}$ (sideband numbers n and m) can be written

$$\begin{aligned} L_{n,m}(m_2, \Delta) = {} & \left\{ K_n K_m + \frac{m_2}{4}(K_{n-1} + K_{n+1}) K_m \sin\Delta + \frac{m_2}{4}(K_{m-1} + K_{m+1}) K_n \sin\Delta \right\} \\ & + j\left\{ -\frac{m_2}{4}(K_{n-1} + K_{n+1}) K_m \cos\Delta - \frac{m_2}{4}(K_{m-1} - K_{m+1}) K_n \cos\Delta \right\}. \end{aligned} \tag{7}$$

In (6), the square root (IM term) of (5) has been developed up to the linear term. Besides the components with indexes $n = \pm 1, \pm 2, \pm 3, \ldots$ and $m = 0$ as well as $n = 0$ and $m = \pm 1, \pm 2, \pm 3, \ldots$ (input tones and harmonics thereof), a large number of combination products will appear in the optical spectrum caused by the nonlinear nature of frequency modulation. This fact, in conjunction with the electrooptical upconversion principle and the subsequent transmission over dispersive fiber, is the reason for the observed intermodulation distortion. Large-signal two-tone laser modulation will of course result in intermodulation distortion also, but the latter is based on other physical principles. Equations (4) and (7) will be further used for several subsequent calculations and derivations.

IV. Electrooptical Upconversion Process

A. Mixing in a Mach–Zehnder Electrooptical Modulator (MZM)

The obtained optical signal due to direct laser modulation is applied to the EOM. The latter is driven at both branches by two out-of-phase sine wave signals ($\pm(m_1/2)\sin\omega_1 t$) of angular frequency ω_1, representing the master oscillator. At the output of the EOM, one can write

$$\begin{aligned} E_{\mathrm{EOM}}(t) = {} & E_1 \tau_{\mathrm{EOM}} \left\{ \sum_{n=-\infty}^{+\infty} L_n \exp j(\omega_0 + n\omega_2)t \right\} \\ & \cdot \left\{ \sum_{r=-\infty}^{\infty} J_r \cos((\delta\Phi_B - \delta\Phi_A + r\pi)/2) \times \exp j(r\omega_1 t) \right\} \\ & \cdot \exp j((\delta\Phi_A + \delta\Phi_B)/2 + \Phi_A) \end{aligned} \tag{8}$$

where τ_{EOM} denotes the modulator transmission coefficient, $\delta\Phi_A$ and $\delta\Phi_B$ the bias induced phase terms of both branches of the modulator, and Φ_A is the phase change due to the physical length of one of both (ideally equally long) interferometer branches. Nominally, in this scheme, the device is operated at minimum transmission bias, which means $(\delta\Phi_B - \delta\Phi_A)/2 = \pm\pi/4, 3\pi/4, \ldots$. The final exponential term in (8) merely represents a phase shift. All Bessel functions are now $J_r = J_r(m_1/2)$ with an EOM index of $m_1/2$ per branch.

B. Fiber Propagation

A simple fiber model is used neglecting polarization-mode dispersion as well as nonlinear fiber effects (short fiber range and low power). A Taylor series development of β and incorporation of the dispersion coefficient (D) leads to the relation for the dispersion propagation constant $-Dc\pi(n\omega_2+r\omega_1)^2/\omega_0^2 = \beta_d(\omega)$. Due to the square in the numerator, the dispersion propagation constant will always be positive and symmetrical around ω_0, i.e., β_d will have the same sign and value for $\omega_0+n\omega_2+r\omega_1$ as for $\omega_0 - n\omega_2 - r\omega_1$, which is an important property with impact on transmission characteristics. The group delay propagation constant β_g can also be gained. Integration of the above yields $(2\pi cD\omega_0^{-1}+k)\cdot(n\omega_2+r\omega_1) = \beta_g(\omega)$ after several steps with k including the integration constants. Since the above propagation factors are a function of ω with $\omega = \omega_0 + n\omega_2 + r\omega_1$ and $\omega_0 = \text{const}$, one can write for the sum

$$\begin{aligned}\beta(r,\,n) &= \beta_0 + \beta_g(\omega(r,\,n)) + \beta_d(\omega(r,\,n))\\ &= \beta_0 + \beta_{g_{r,n}} + \beta_{d_{r,n}}\\ &= \beta_{r,n}.\end{aligned} \tag{9}$$

A kind of index annotation is possible at this point, since discrete spectral lines are considered. The phase shift $\varphi = -\beta\cdot l$ due to fiber transmission over length l, experienced by an arbitrary sideband r, n, can now be expressed and incorporated into (9), which will then read at the fiber output interface

$$\begin{aligned}E_L(t) = \Bigg\{ &\sum_{r=-\infty}^{+\infty}\sum_{n=-\infty}^{+\infty}\left[J_r\cos\left(\frac{\delta\Phi_B-\delta\Phi_A}{2}+r\frac{\pi}{2}\right)\right]\\ &\cdot [L_n]e^{j(\omega_0+r\omega_1+n\omega_2)t}e^{-j\beta_{r,n}l}\Bigg\}\\ &\times E_1\tau_{\text{EOM}}e^{j((\delta\Phi_A+\delta\Phi_B)/2+\Phi_A)}e^{-al}.\end{aligned} \tag{10}$$

The attenuation term within the propagation function $\gamma(\omega) = \alpha+j\beta(\omega)$ is assumed to be constant over frequency and appears as a common amplitude factor.

C. Bandpass Filtering

Optical demultiplexers of a practical system are substituted by bandpass filters in the model. The transfer function $Gf(\omega)$ of the filter (OBPF) is set equivalent to that of the diplexer's "in/drop" two port section. Then,

$$\begin{aligned}G_{fr,n} &= G_f(\omega(r,\,n))\cdot\delta(\omega-\omega_0-r\omega_1-n\omega_2)\\ &= |G_{fr,n}|\cdot e^{j\varphi f_{r,n}}\cdot\delta(\omega-\omega_0-r\omega_1-n\omega_2).\end{aligned} \tag{11}$$

This definition is possible since the input frequencies into the filter are known and can be described by the indexes n and r. Then, after performing $E_{\text{PD}}(\omega)+E_L(\omega)\cdot G_F(\omega)$ and retransformation, the expression

$$\begin{aligned}E_{\text{PD}}(t) = \Bigg\{ &\sum_{r=-\infty}^{+\infty}\sum_{n=-\infty}^{+\infty}\left[J_r\cos\left(\frac{\delta\Phi_B-\delta\Phi_A}{2}+r\frac{\pi}{2}\right)\right]\\ &\cdot[L_n]|G_{f_{r,n}}|e^{-j\beta_{r,n}l}e^{j\varphi f_{r,n}}\times e^{j(\omega_0+r\omega_1+n\omega_2)t}\Bigg\}\\ &\cdot E_1\tau_{\text{EOM}}e^{j((\delta\Phi_A+\delta\Phi_B)/2+\Phi_A)}e^{-al}\end{aligned} \tag{12}$$

will denote the time-dependent, filtered optical field prior to photodetection.

D. Photodetection Process

The photodetected current is gained by performing, $i_{\text{PD}}(t) = A_2\cdot E_{\text{PD}}(t)\cdot E_{\text{PD}}(t)^*$, where A_2 denotes the optoelectric conversion factor. Considering the previously derived expression for $E_{\text{PD}}(t)$, a large number of terms at all combination frequencies will result, even for a limited range of r and n. Hereof, the most relevant products are: $2\omega_1+\omega_2$, upper sideband (USB) downlink signal at 60.0 GHz; $2\omega_1-\omega_2$, lower sideband (LSB) image at 55.2 GHz; $2\omega_1$, local oscillator (doubled master tone) at 57.6 GHz. The figures denote the corresponding frequency as has been used in the experimental system. After several algebraic operations, which have to be omitted here, one obtains an expression for the complex envelope of the USB

$$\begin{aligned}\overline{i_{\text{USB}}} = E_1^2A_2\tau_{\text{EOM}}^2e^{-2al}\cdot &\sum_{r=-\infty}^{+\infty}-J_rJ_{r+2}\\ &\cdot\cos^2\left(\frac{1}{2}(\delta\Phi_B-\delta\Phi_A)+\frac{1}{2}r\pi\right)\\ &\times\sum_{n=-\infty}^{+\infty}2\Bigg\{|[L_n][L_{n+1}]^*G_{fr,n}G_{fr+2,n+1}|\\ &\cdot\exp -j\arg\Big([L_n][L_{n+1}]^*|G_{fr,n}|\\ &\times|G_{fr+2,n+1}|\\ &\cdot\exp j(\varphi_{r,n}\\ &-\varphi_{r+2,n+1})\Big)\Bigg\}\end{aligned} \tag{13}$$

with $\varphi_{r,n} = -\beta_{r,n}l+\varphi_{f_{r,n}}$. It is possible to modify the indexes, namely $n+1$ to $n-1$, to represent the LSB. Also, if $n+1$ is changed to n, the generated current of the doubled master oscillator is described. Considering (13), several simplifications can be made. Since $L_n\cdot L_{n+1}^*$ is complex, one can write for the first exponential function

$$\begin{aligned}&\exp -j\arg\Big([L_n][L_{n+1}]^*|G_{fr,n}||G_{fr+2,n+1}|\\ &\qquad\cdot\exp j(\varphi_{r,n}-\varphi_{r+2,n+1})\Big)\\ &=\exp -j\begin{Bmatrix}\arg([L_n][L_{n+1}]^*)\\ +(\varphi_{fr,n}-(\beta_0+\beta_{g_{r,n}}+\beta_{d_{r,n}})l)\\ -(\varphi_{fr+2,n+1}-(\beta_0+\beta_{g_{r+2,n+1}}+\beta_{d_{r+2,n+1}})l)\end{Bmatrix}.\end{aligned} \tag{14}$$

It can be shown that, because we have a ratio of angular frequencies in β_g in linear form, the involved expressions will, for any value of n and r, be independent of those indexes. One can separate a phase term from the exponent of the e-function

$$\begin{aligned}&\exp -j\begin{Bmatrix}\arg([L_n][L_{n+1}]^*)\\ +(\varphi_{fr,n}-(\beta_0+\beta_{g_{r,n}}+\beta_{d_{r,n}})l)\\ -(\varphi_{r+2,n+1}-(\beta_0+\beta_{g_{r+2,n+1}}+\beta_{d_{r+2,n+1}})l)\end{Bmatrix}\\ &=\exp -j\left\{\arg([L_n][L_{n+1}]^*)+(\varphi_{fr,n}-\varphi_{fr+2,n+1})\right.\\ &\qquad\left.-(\beta_{d_{r,n}}-\beta_{d_{r+2,n+1}})l\right\}\cdot\exp -j\beta_{g_{2,1}}l\end{aligned} \tag{15}$$

and also further from the sums over n as well as over r of the complete expression in (13). On the contrary, the same operation cannot be performed for β_d. The square involved in the definition prevents this term from being independent of n and r.

V. Results and Discussion

An ideal WDM channel filter is assumed in the following, mainly in order to reduce the amount of variables and parameters in the considerations, i.e., $|G_f| = 1$ and $d\varphi_f/d\omega = \text{const}$, in the range $\omega_0 - \omega_1 - 10\omega_2 \leq \omega \leq \omega_0 + \omega_1 + 10\omega_2$ and 0 elsewhere. In the expressions provided in the previous section, an arbitrary filter function can be inserted.

Equation (13) in conjunction with (15) will now be discussed. In all examples discussed below, the frequency range is chosen to be the same as in the experimental system of [9]: $\omega_2/2\pi = 2.400$ GHz and $\omega_1/2\pi = 28.800$ GHz. Also, $D = 16.2$ ps/(nm·km) and, for simplicity, $\alpha = 0$. A 10-GBit/s multiquantum-well (MQW)–distributed feedback (DFB) laser diode has been used (NEL model NLK1551HSC). At ω_2, the device exhibited a chirp factor $\alpha_{\text{chirp}} = 4.1$ and an IM-to-FM angle $\Delta = 1.3$ rad.

A. Amplitude Linearity

Output power P_{USB} of the upper sideband at 60 GHz versus power at the input-IF (according to $P_{\text{IF,in}} \sim m_2^2$) is considered. Cases will be compared for different chirp values and different phase angles Δ and the curves are normalized according to

$$P_{\text{USB}}^{(\text{norm.})}(l, m_{2}...) = \frac{P_{\text{USB}}(l, m_{2}...) \cdot m_{2,\text{lin}}^2}{P_{\text{USB}}(l = 0, m_{2,\text{lin}}...)} \qquad (16)$$

in order to improve overview, such that a 0-dB relative output power results for a unity modulation index $m_2(\log) = 0$ dB for the ideally linear case ($l = 0$ km). The value $m_{2,\,\text{lin}}$ represents linear conditions and is sufficiently small ($m_{2,\,\text{lin}} = 0.1$ in the given case).

For short fiber transmission lengths l <2 km, linear conditions are prevailing but noticeable compression begins shortly above that range. At $l = 6$ km, strong compression and, in addition, a turnover point after which the output power is inverse to input can be observed for a chirp of $\alpha_{\text{chirp}} = 4.1$ for all considered values of Δ [see Fig. 3(a)]. The power difference between $|\Delta| = 0$ and $|\Delta| = \pi$ is in excess of 13 dB for $\alpha_{\text{chirp}} = 2$. For $l = 12.8$ km, as shown in Fig. 3(b), the turnover point now begins to appear for smaller chirp values ($\alpha_{\text{chirp}} = 1$) and has shifted toward lower $m_2 (m_2 \approx 0.3)$ for $\alpha_{\text{chirp}} = 4.1$. The power difference (in decibels) for both chirp values due to varying Δ-angles is somewhat reduced. However, this is only valid until the (first) turnover point. Thereafter, one can observe a very steep (≈40 dB) power drop for $P_{\text{USB}}(\alpha_{\text{chirp}} = 4.1, \Delta = 0, \ldots)$ and $P_{\text{USB}}(\alpha_{\text{chirp}} = 4.1, \Delta = \pi, \ldots$ while only a ≈10-dB drop for $P_{\text{USB}}(\alpha_{\text{chirp}} = 4.1, \Delta = \pi/2, \ldots)$ with a much smoother minimum. The example again underlines the importance of the knowledge of angle Δ in order to precisely determine and predict the detected power over the whole range. If transmission length is further increased to between $l = 25$ km and $l = 30$ km, a power collapse will appear twice for $\alpha_{\text{chirp}} = 4.1$, and, quantitatively to a much larger extent for $\alpha_{\text{chirp}} = 2$.

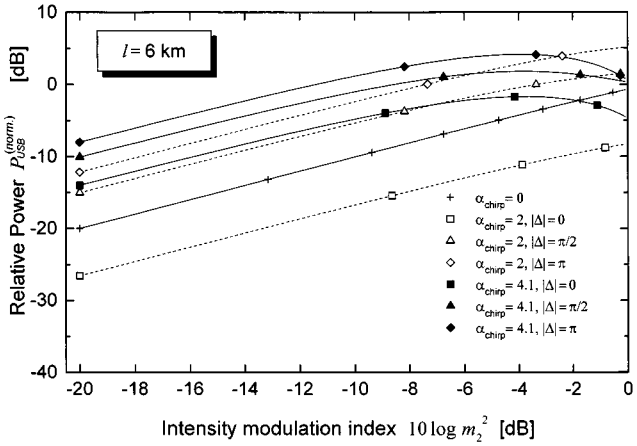

(a)

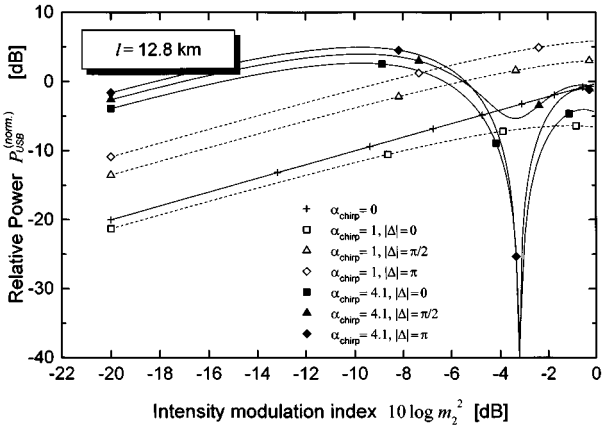

(b)

Fig. 3. Calculated normalized detected power $P_{\text{USB}}^{(\text{norm.})}$ as a function of square of intensity modulation index $(m_2^2(\log))$ for fiber lengths (a) $l = 6$ and (b) 12.8 km and different values of α_{chirp} and $|\Delta|$.

Being of practical value, a gain compression of typically $G_C = -1$ dB is specified in microwave and millimeter-wave systems. The graphs to follow depict the calculated value of laser diode intensity modulation index m_2 in logarithmic form versus fiber transmission length of $l = 0, \ldots, 58$ km for which this gain compression condition will be reached. Angle Δ and α_{chirp} are curve parameters, traces are interrupted if the condition cannot be met, even if $m_2 = 1$ is required at the input.

In Fig. 4(a), for the case of ideal blue shift ($\Delta = 0$), one can observe a very steep decrease for $\alpha_{\text{chirp}} = 4.1$ of usable drive level and only $m_2(\log) = -14.2$ dB lead to a 1-dB gain compression at the output at $l = 2$ km, the curve continues to fall and eventually reappears at $m_2(\log) = 0$ dB after $l = 3$ km. Then, it again decays at a slower rate and goes through a minimum of approximately −20 dB at $l \approx 28$ km. Similar behavior is also observed for $\alpha_{\text{chirp}} = 2$ and $\alpha_{\text{chirp}} = 1$. Here, the first curve discontinuities appear at somewhat higher lengths: the smooth minima are also found around approximately $l = 25$ km but they are higher in magnitude. Clearly, from these facts, it seems difficult to design a radio-optical link with this set of parameters. Unless the link is exceptionally short (a few hundred meters), sensitivity to fiber length variation is very high

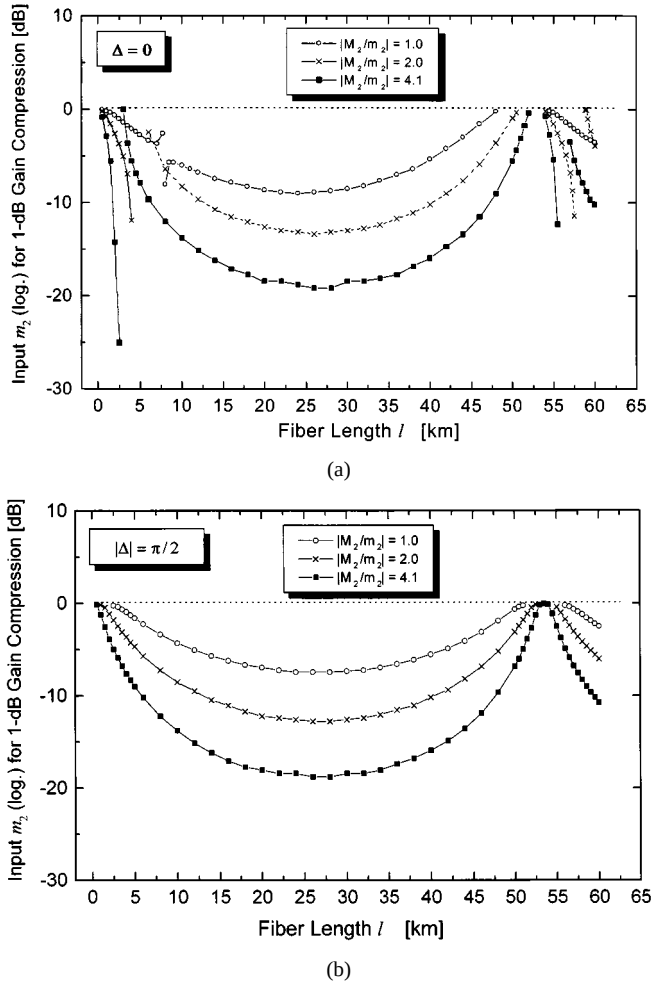

Fig. 4. Input intensity modulation index $m_2^2(\log)$ resulting in 1-dB gain compression ($G_c = -1$ dB) at output as function of fiber length l for different values of α_{chirp} with (a) $|\Delta| = 0$ and (b) $|\Delta| = \pi/2$.

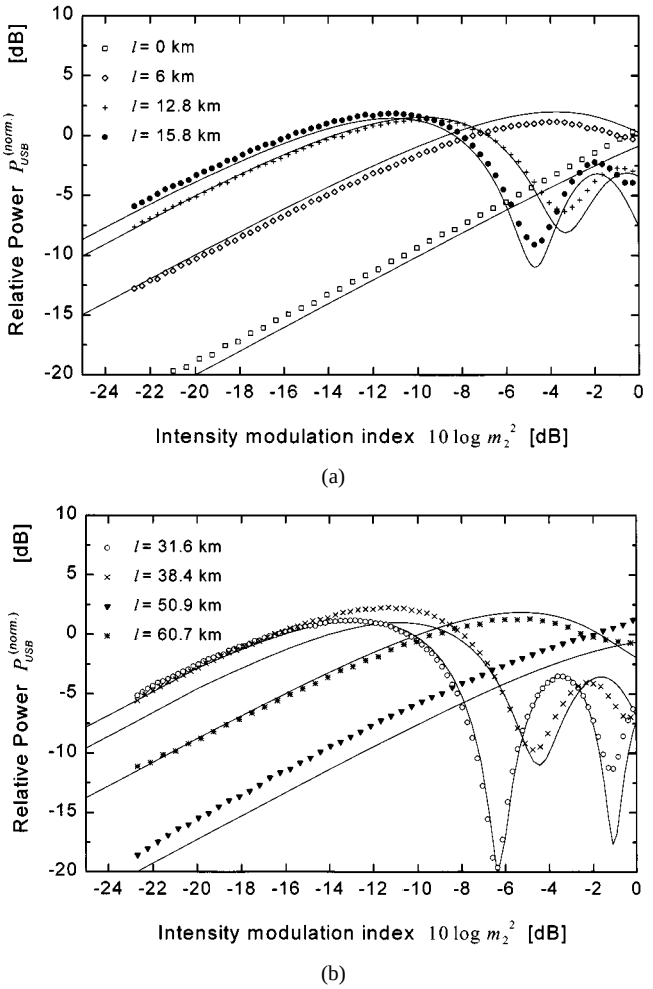

Fig. 5. Measured and calculated (−) detected power $P_{\text{USB}}^{(\text{norm})}$ as a function of square of intensity modulation index $(m_2^2(\log))$ for fiber lengths: (a) $l = 0,\ 6,\ 12.8,\ 15.8$km (□, ◇, +, •) and (b) $l = 31.6,\ 38.4,\ 50.9,\ 60.7$ km (○, ×, ▼, ∗).

at short distances of a few kilometers, which is highly undesirable. The medium length region ($l = 15, \ldots, 35$ km) offers a more flat response but suffers from limitation in dynamic range (low usable m_2). In the second example of Fig. 4(b), the condition $|\Delta| = \pi/2$ is considered. There are no discontinuities, and the 1-dB gain drop occurs for much higher (and thus usable) values of m_2 for the first few kilometers of fiber link. Even for the highest given chirp of $\alpha_{\text{chirp}} = 4.1$, a value of $m_2(\log) = -3$ dB is obtained after $l = 3.5$ km. Therefore, unlike the previous case, design and realization of a radio-optical link for the given parameters seems less critical, since the first kilometers of fiber can be used with only a small sacrifice in performance. In terms of range, this is likely to be sufficient for the intended indoor application. The minima in the medium length region ($L = \ldots, 35$ km) and the properties around $l = 50$ km are similar to the case of $\Delta = 0$.

Measurements: Eight curves depicting the input—to-output power relationship are shown in Fig. 5 for $l = 0, \ldots, 60.7$ km at $\omega_2/2\pi = 2.4$ GHz. The previously mentioned normalization has been applied. Even for moderate to high values of $m_2(m_2(\log) < -3$dB), good agreement is found which is interesting considering the small-signal model of the laser diode.

B. Phase Linearity

Considering the nonlinear properties, the magnitude of the detected millimeter-wave signal at USB similar behavior can also be expected for the nonlinear phase response ϑ of the photocurrent. The complex envelope of the detected current $\overline{i_{\text{USB}}}$ has been derived in (13). Let the considered function be $\overline{i_{USB}} = f(m_2, \alpha_{\text{chirp}}, \Delta, l)$ and absolute phase, which is not of interest, is eliminated applying the expression

$$\begin{aligned}\varphi_{\text{USB}}(m_2, l, \alpha_{\text{chirp}}, \Delta) &= \arg\left[\overline{i_{\text{USB}}}(m_2, l, \alpha_{\text{chirp}}, \Delta)\right] \\ &\quad - \arg\left[\overline{i_{\text{USB}}}(m_{2,\text{lin}}, l, \alpha_{\text{chirp}}, \Delta)\right]. \end{aligned} \tag{17}$$

Preferably, $m_{2,\text{lin}}$ has to be very small ($m_{2,\text{lin}} = 0.1$ is sufficient here). In addition to that, initially, the important condition $\omega_0(m_2) = \text{const.}$ shall be fulfilled. Observing Fig. 6(a) and (b), a noticeable difference from the previously considered amplitude properties is that now it is not sufficient to include $|\Delta|$ as a parameter. Rather, as can be seen, the sign of Δ is of major importance and this is the reason for including a higher number of

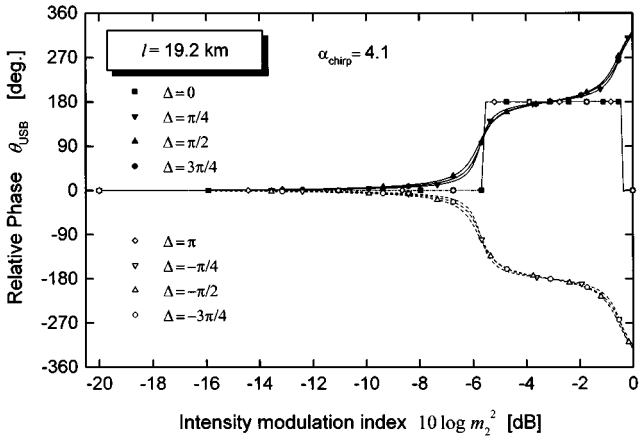

(a)

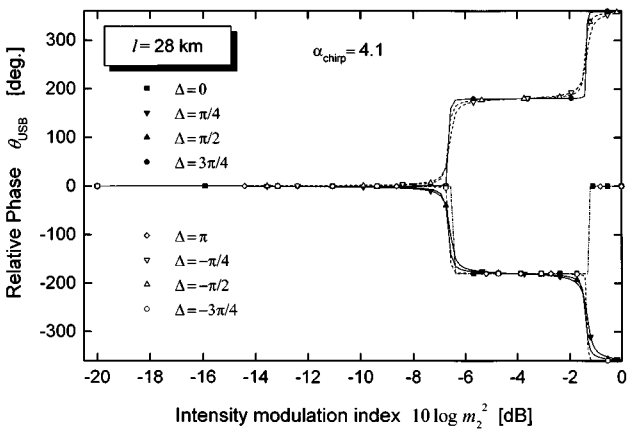

(b)

Fig. 6. Relative phase ϑ_{USB} as a function of square of intensity modulation index $(m_2^2(\log))$ for fiber length: (a) $l = 19.2$ km and (b) $l = 28$ km, $\alpha_{\mathrm{chirp}} = 4.1$, and different Δ-values.

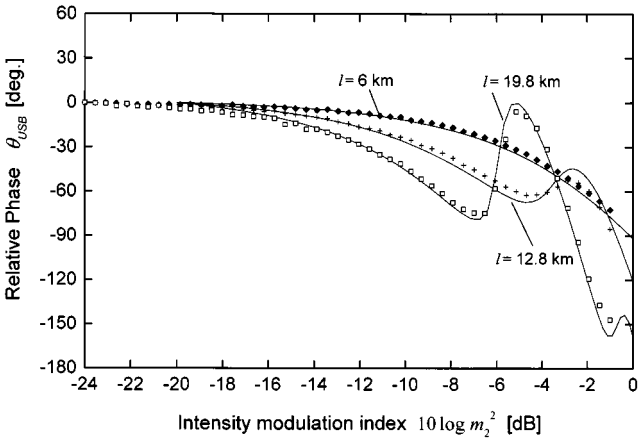

(a)

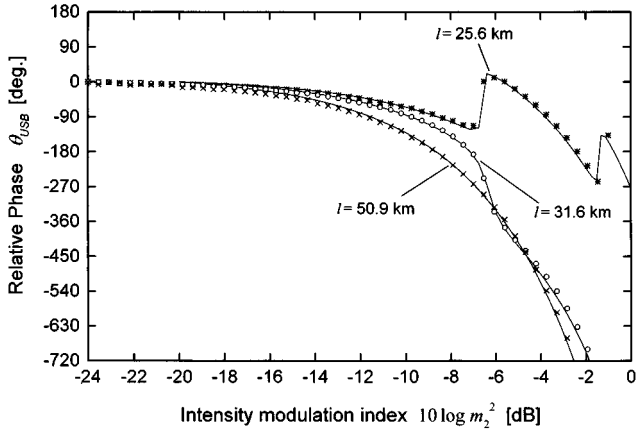

(b)

Fig. 7. Measured and calculated $(-)$ relative phase ϑ as a function of square of intensity modulation index $(m_2^2(\log))$ for fiber lengths: (a) $l = 6, 12.8$, and 19.8 km ($\blacklozenge$, $+$, $\square$) and (b) $l = 25.6, 31.6$, and 50.9 km ($*$, $\bigcirc$, $\times$).

example parameters. Since $\vartheta_{\mathrm{USB}}(\Delta, \ldots) = -\vartheta_{\mathrm{USB}}(-\Delta, \ldots)$ is valid, it is important to note that, if laser diode parameter extraction is of interest, measurement of detected current phase for this method (and topology) can in fact reveal the sign of Δ [12].

As expected, nonlinear phase distortion ϑ_{USB} is strongest for those fiber lengths l where amplitude compression is strong. Also, ideal blue-shift ($\Delta = 0$) and red-shift ($\Delta = \pi$) phase compression is $\vartheta_{\mathrm{USB}} = 0$ for both cases unless there is an associated amplitude notch over m_2. Such notches are particularly (infinitely) deep for the given values of Δ and discrete phase jumps occur, then $\vartheta_{\mathrm{USB}}(m_2, \ldots) = 0, +180^\circ$ or -180°.

Measurements: Six measurements are depicted in Fig. 7 for laser diode device LD1 (10-GBit/s MQW–DFB laser) at an operating frequency of $\omega_2/2\pi = 2.4$ GHz, where $\alpha_{\mathrm{chirp}} = 4.1$ and $\Delta = 1.3$. The derivations of the previous section have been based on the relationship $\omega_0(m_2) = \mathrm{const}$. However, in this experiment, the laser center frequency ω_0 showed a drift with increasing modulation current envelope (it is important to note that the envelope rather than the current swing is meant). Thereby, the modulation spectrum remains unchanged. By means of a separate measurement for this device, a curve fit could be obtained: $\omega_0(m_2) \cong \omega_0(0) - 2\pi(0.767m_2 + 8.232m_2^2)$ GHz. It has then been incorporated into the expressions for β_g and β_d. Good agreement is found in the experiment. The (superimposed) negative slope due to $\omega_0(m_2)$ is obvious but the previously described characteristics are also clearly visible. The phase transitions become steeper for higher l. Also, it is interesting to observe the different signs of the phase change, which is positive for $l = 25.6$ km but negative for $l = 31.6$ km (both at $m_2 \approx -6$ dB). Theory predicts this effect (for example, at close values of $l = 19.2$ km and $l = 28$ km with $\Delta = \pi/2$).

C. Intermodulation Distortion

The two-tone intermodulation distortion of third and fifth order will be discussed next. Results on the obtained level of intermodulation distortion for fixed intensity modulation indexes versus fiber length have been first presented in [13]. In this section, an analytical expression will be provided, and the theoretical and measured behavior with a variable parameter m_2 as well as the resulting input intercept points for variable fiber span will be shown. Equation (8) is used and the indexes of phase terms β and the filter transfer function G_f are extended $(r, n) \rightarrow (r, n, m)$. The analytical approach is identical to the one of the single tone (as described in Section

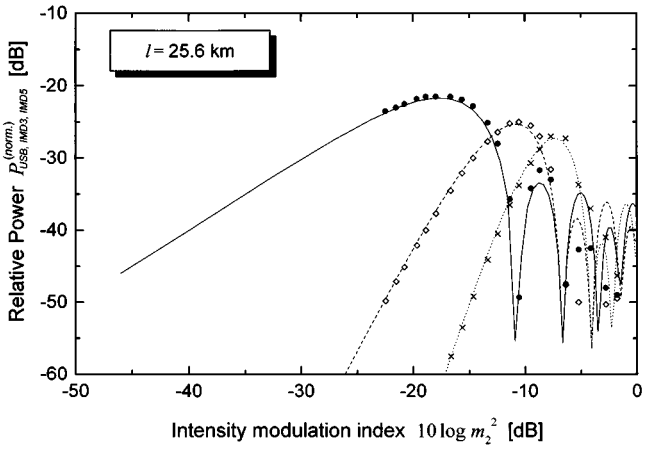

Fig. 8. Normalized detected power $P^{(\mathrm{norm.})}_{\mathrm{USB,IMD3,IMD5}}$ as a function of square of intensity modulation index $(m_2^2(\log))$ for fiber length $l = 25.6$ km. Measured (•, ◇, ×) and calculation (solid, dashed, points) for USB, IMD3, and IMD5.

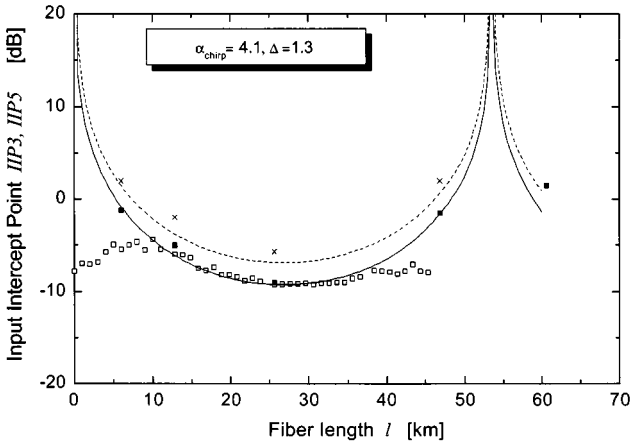

Fig. 9. Measured and calculated Input Intercept Points IIP3 and IIP5 versus fiber length. Lines are calculated data (solid, dashed), and symbols are measurements (□: experiment 1; ■, ×: experiment 2) for IIP3 and IIP5, respectively.

IV) but involves somewhat more extensive algebra. Only the result can be shown here, as seen in (18) at the bottom of this page, where x identifies the product addressed by the variable u. In the following order, the lower side fifth-order product ($\mathrm{IMD5}^{(a)}$) is defined for $u = 3$, the lower side third order product ($\mathrm{IMD3}^{(a)}$) for $u = 2$, and so forth.

Measurements: The modulation frequencies set are again as $\omega_2^{(a)}/2\pi = 2.399$ GHz and $\omega_2^{(b)}/2\pi = 2.401$ GHz. The following normalization with $m_{2,\mathrm{lin}} = 0.01$ applies in order to improve the overview such that an ideally linear response will lead to a relative output power of 0 dB for full modulation $m_2^2(\log) = 0$ dB: $P_x^{(\mathrm{norm.})}(l, m_2, \ldots) = P_x(l, m_2 \ldots) \cdot m_{2,\mathrm{lin}}^2 / P_{\mathrm{USB}}(l, m_{2,\mathrm{lin}} \ldots)$. In Fig. 8 ($l = 25.6$ km), it can be seen that intermodulation products can also experience multiple power dips and alternating maxima and minima visualize the spectral energy transfer. Experimental data fit well with the calculated results. Again, agreement is found for comparably high m_2-values. Also, in Fig. 9, denoting the input related intercept points (third and fifth order) after approximately $l = 8$ km, very good agreement between calculation and measurements of experiment 1 as well as experiment 2 is found. The limited dynamic range available in experiment 1 led to poor results for intermodulation product magnitude and limits extrapolation accuracy below this length, as opposed to experiment 2 which still provided very good results at $l = 6$ km, for higher lengths as well as for IIP5.

VI. Conclusion

The combined effects of laser chirp, electrooptical mixing, dispersive fiber transmission, and photodetection on the nonlinear signal properties of the generated millimeter-wave signal have been described. A single optical channel of a WDM system has been considered including its demultiplexing filters. Analytical formulations, highly applicable for practical purposes, expressing the complex currents of fundamental and higher order products are provided for the case of single- and two-tone modulation. The involved behavioral model of the laser diode is straightforward and requires a limited set of parameters. In order to predict resulting signals precisely, essential for system design calculations, exact knowledge of laser diode chirp magnitude and particularly of its argument (IM-to-FM phase lag) is essential. Several examples with variable parameters have been shown and discussed. The established link model performed well, even under moderate to large signal conditions, and very good agreement has been achieved between theory and experiment.

$$\begin{aligned}\overline{i_x} = E_1^2 A_2 \tau_{\mathrm{EOM}}^2 e^{-2\alpha l} \cdot \sum_{r=-\infty}^{+\infty} -J_r J_{r+2} \cos^2\left(\frac{1}{2}(\delta\Phi_B - \delta\Phi_A) + \frac{1}{2} r\pi\right) \\ \times \sum_{z=-\infty}^{+\infty} \sum_{n=-\infty}^{+\infty} 2\Big\{ |[L_{n,-(z+1)-n}][L_{n+u,-(z+u)-n}]^* G_{fr,n,-(z+1)-n} G_{fr+2,n+u,-(z+u)-n}| \\ \times \exp -j \arg\Big([L_{n,-(z+1)-n}][L_{n+u,-(z+u)-n}]^* |G_{fr,n,-(z+1)-n}||G_{fr+2,n+u,-(z+u)-n}| \\ \times \exp j(\varphi_{r,n,-(z+1)-n} - \varphi_{r+2,n+u,-(z+u)-n})\Big)\Big\} \end{aligned} \tag{18}$$

REFERENCES

[1] G. J. Simonis and K. G. Purchase, "Optical generation, distribution and control of microwaves using laser heterodyne," *IEEE Trans. Microwave Theory Tech.*, vol. 38, pp. 667–669, May 1990.

[2] D. Novak, Z. Ahmed, R. B. Waterhouse, and R. S. Tucker, "Signal generation using pulsed semiconductor lasers for application in millimeter-wave wireless links," *IEEE Trans. Microwave Theory Tech.*, vol. 43, pp. 2257–2262, Sept. 1995.

[3] C. G. Schäffer, R. P. Braun, G. Grosskopf, F. Schmidt, and M. Rohde, "Microwave multichannel system with a sideband injection locking scheme in the 60 GHz-band," in *IEEE Int. Microwave Photon. Conf.*, Princeton, NJ, Oct. 1998, pp. 67–69.

[4] T. Kuri, K. Kitayama, and Y. Ogawa, "A novel fiber-optic millimeter wave uplink incorporating 60 GHz photonic downconversion with remotely fed optical pilot tone using an electro-absorption modulator," in *IEEE Int. Microwave Photon. Conf.*, Princeton, NJ, Oct. 1998.

[5] T. Berceli, "A new approach for optical millimeter wave generation utilizing locking techniques," in *IEEE MTT-S Int. Microwave Symp. Dig.*, Denver, CO, June 1997, pp. 1721–1724.

[6] M. Sauer, K. Kojucharow, H. Kaluzni, and W Nowak, "RF-front end and optical feeding system for a millimeter-wave broadband communications system at 60 GHz," in *SBMO/IEEE MTT-S Int. Microwave Optoelectron. Conf.*, vol. 1, Natal, Brazil, 1997, pp. 227–232.

[7] K. Kitayama and A. Stöhr *et al.*, "An approach to single optical component antenna base stations for broad-band millimeter-wave fiber-radio access systems," *IEEE Trans. Microwave Theory Tech.*, vol. 48, pp. 2588–2595, Dec. 2000.

[8] D. Wake, L. Noel, D. Moodie, D. Marcenac, L. Westbrook, and D. Nesset, "A 60 GHz 120Mb/s QPSK fiber radio transmission experiment incorporating an electroabsorption modulator transceiver for a full duplex optical data path," in *IEEE MTT-S Int. Microwave Symp. Dig.*, Denver, CO, June 1997, pp. 39–42.

[9] K. Kojucharow, M. Sauer, H. Kaluzni, D. Sommer, F. Poegel, W. Nowak, A. Finger, and D. Ferling, "Simultaneous electro-optical upconversion, remote oscillator generation and air transmission of multiple optical WDM channels for a 60 GHz high capacity indoor system," *IEEE Trans. Microwave Theory Tech.*, vol. 47, pp. 2249–2256, Dec. 1999.

[10] I. N. Bronstein and K. A. Semendjajew, *Taschenbuch der Mathematik*. Leipzig: Teubner-Verlag, 1979.

[11] G. J. Meslener, "Chromatic dispersion induced distortion of modulated monochromatic light employing direct detection," *IEEE J. Quantum Electron.*, vol. QE-20, pp. 1208–1216, Oct. 1984.

[12] E. Peral and A. Yariv, "Large signal theory of the effect of dispersive propagation on the intensity modulation response of semiconductor lasers," *J. Lightwave Technol.*, vol. 18, pp. 84–89, Jan. 2000.

[13] M. Sauer, K. Kojucharow, H. Kaluzni, and M. Otto, "Impact of laser chirp on carrier and IMD power in electro-optical upconverted millimeter-wave fiber optic links," *Electron. Lett.*, vol. 35, no. 10, pp. 834–836, 1999.

[14] G. Agrawal, "Power spectrum of semiconductor lasers: Chirp induced fine structure," *IEEE J. Quantum Electron.*, vol. QE-21, pp. 680–686, June 1985.

[15] ——, "Power spectrum of semiconductor lasers: Chirp induced fine structure," *IEEE J. Quantum Electron.*, vol. QE-21, p. 1845, June 1985.

Konstantin Kojucharow (S'98) was born in Eisleben, Germany, in 1970. He received the Dipl.-Ing. degree in microwave techniques from the Dresden University of Technology, Dresden, Germany, in 1995, and is currently working toward the Ph.D. degree at the Dresden University of Technology.

He spent six month as an exchange student at North Carolina State University, Raleigh, where he was involved with microwave quasi-optical systems. His research interests include low-noise amplifiers and devices, millimeter-wave communications systems, and analog radio-optical links. While conducting his doctoral studies, he also works with IRK Dresden, Dresden, Germany, a microwave and antenna development company. He also serves as a consultant.

Mr. Kojucharow is a member of the IEEE Microwave Theory and Techniques Society (IEEE MTT-S).

Michael Sauer (A'96–M'96) was born in Dresden, Germany, on February 17, 1970. He received the Dipl.-Ing. degree in electrical engineering and the Ph.D. degree from the Dresden University of Technology, Dresden, Germany, in 1994 and 2000, respectively.

In January 2001, he joined Corning Inc., Corning, NY. His research interests include fiber Bragg gratings, generation and fiber-optic transmission of millimeter-wave signals, and architectures of millimeter-wave communications systems.

Dr. Sauer is a member of the IEEE Lasers and Electro-Optics Society (IEEE LEOS).

Christian Schäffer (S'96–M'98), photograph and biography not available at the time of publication.